

# Catalysis Science & Technology

Accepted Manuscript



This is an *Accepted Manuscript*, which has been through the Royal Society of Chemistry peer review process and has been accepted for publication.

*Accepted Manuscripts* are published online shortly after acceptance, before technical editing, formatting and proof reading. Using this free service, authors can make their results available to the community, in citable form, before we publish the edited article. We will replace this *Accepted Manuscript* with the edited and formatted *Advance Article* as soon as it is available.

You can find more information about *Accepted Manuscripts* in the [Information for Authors](#).

Please note that technical editing may introduce minor changes to the text and/or graphics, which may alter content. The journal's standard [Terms & Conditions](#) and the [Ethical guidelines](#) still apply. In no event shall the Royal Society of Chemistry be held responsible for any errors or omissions in this *Accepted Manuscript* or any consequences arising from the use of any information it contains.

## Decomposition of Methyl Species on a Ni(211) surface: Investigations of the Electric Field Influence

Fanglin Che,<sup>a</sup> Alyssa J. Hensley,<sup>a</sup> Su Ha,<sup>a</sup> Jean-Sabin McEwen<sup>\*a,b,c</sup>

<sup>a</sup>*The Gene and Linda Voiland School of Chemical Engineering and Bioengineering, Washington State University, WA, 99164*

<sup>b</sup>*Department of Physics and Astronomy, Washington State University, Pullman, WA, 99164*

<sup>c</sup>*Department of Chemistry, Washington State University, Pullman, WA, 99164*

### Abstract

Density functional theory calculations are performed to examine how an external electric field can alter the reaction pathways on a stepped Ni(211) surface with regards to the decomposition of methyl. We compare our results to those previously obtained on a close-packed Ni(111) surface and a bimetallic Au/Ni surface. The structures, adsorption energies, and reaction energy barriers of all methyl species on the Ni(211) surface are identified. The calculated results indicate that the presence of an external electric field not only alters the site preferences for the adsorbates on Ni(211), but also significantly changes the adsorption energies of the CH<sub>x</sub> species. By comparison with our previous results, this electric field effect is smaller than that on Ni(111). The local electric field value is also found to differ at the various adsorption sites for the CH<sub>3</sub> group on Ni(211). From the results, a correlation between the calculated local electric fields, the adsorption energies and effective dipole moments values is investigated. The calculations also show that the stepped surfaces are more reactive for the elementary dissociation reactions of the CH<sub>x</sub> species as compared to the Ni(111) surface. The final conclusion is that a positive electric field strengthens the adsorption energy of reactant CH<sub>3</sub>, increases the energy barriers of the decomposition of CH<sub>x</sub> species and weakens the adsorption energies of C and H. This suggests that the formation of pure C atoms deposits will be impeded by an external positive electric field.

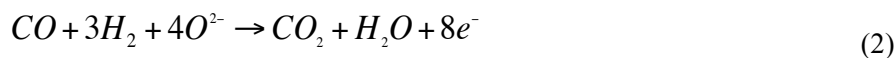
**Keywords:** *external electric field, methyl decomposition, coke formation, Ni(211), Ni(111), DFT*

---

\* Corresponding author: [js.mcewen@wsu.edu](mailto:js.mcewen@wsu.edu) (J.-S. McEwen)

## 1 Introduction

Solid oxide fuel cells (SOFC) offer a clean technology that electrochemically converts chemical energy of fuels, such as petrochemical derived hydrocarbons and biomass derived oxygenated hydrocarbons, directly into electrical energy. This fuel cell technology provides several potential advantages over traditional gas turbine engine technologies, including high electrical efficiency, fuel flexibility, and low emission of pollutants.<sup>1,2</sup> Methane is the simplest and most widely available hydrocarbon of the natural gas fuels and can be regarded as a renewable energy resource if derived from anaerobic digestion.<sup>3-5</sup> Nowadays, there is a great interest in the SOFC operation using this biomass-derived methane fuel.<sup>6</sup> Typically three routes are available for operating on methane fuel in a SOFC, including direct electrochemical conversion, external reforming and internal reforming.<sup>7-9</sup> Usually, one operates the SOFC with a Ni-based anode<sup>10, 11</sup> because of its economic advantages, great conductivity and high catalytic activity for electrochemical oxidation of hydrogen and carbon monoxide (i.e., syngas).<sup>12</sup> In SOFCs, the steam reforming reaction of methane species over Ni catalysts is one possible method to produce hydrogen and synthesis gas (Eq. (1)). The resulting CO and H<sub>2</sub> products can then be electrochemically oxidized by reacting with lattice oxygen at the Ni-based anode with accompanied release of electrons (Eq. (2)).<sup>13-15</sup> These electrons are carried back from the anode to the cathode via an external circuit, completing the electric current loop.<sup>16</sup>



However, before the SOFC system can be widely used for the commercial market, there are several significant issues that need to be addressed. Although the stepped Ni surface shows high activity and efficiency in steam reforming reaction processes, the main disadvantage of using a stepped Ni surface for this reaction is that carbon deposits are easily formed on stepped sites, which can rapidly deactivate the Ni catalysts and destabilize the industrial operations.<sup>17, 18</sup> Therefore, the suppression of coke formation over a Ni stepped surface is actively studied by theoretical and experimental researchers.<sup>19, 20</sup> Theoretically, Benggaard et al.<sup>17</sup> investigated the steam reforming and the nucleation of graphite reactions over both Ni(111) and Ni(211) surfaces. For these two reactions, it is clearly seen that the Ni(211) surfaces are more active than the Ni(111) surfaces. In addition, they suggested that various kinds of additives, such as potassium, sulfur, and gold on Ni surfaces, preferentially bind to the step edges of Ni resulting in a reduced formation of coke. Huang et al.<sup>20</sup> presented a detailed density functional theory (DFT) study of the dissociation of CH<sub>x</sub> (x=1~4) on Au-alloyed Ni(211) surfaces, considering different ratios of

Au atoms to the total number of stepped Ni atoms. Their results showed that a small addition of Au greatly hampered the formation of carbon, while increasing the amount of Au on a Ni catalyst can only slightly hinder the dissociation of  $\text{CH}_x$ . Moreover, other researchers have also used Cu,<sup>18</sup> Rh,<sup>21</sup> Ru,<sup>22</sup> Pt,<sup>23</sup> Ag<sup>19</sup> and Pd<sup>24</sup> as promoters to increase the coke resistance of pure Ni catalysts. Experimentally, Nikolla et al.<sup>2</sup> introduced Sn into Ni to synthesize a Ni/Sn surface alloy (0.5–1 wt % nominal loading of Sn with respect to Ni) in order to improve the carbon tolerance in the steam reforming reaction. The results showed that carbon atoms on a Ni/Sn surface preferred to be oxidized rather than to form carbon-carbon bonds. Nielsen et al.<sup>25</sup> provided evidence that adsorbed Au had a strong tendency to incorporate into the first Ni (110) layer rather than into the bulk through scanning tunneling microscopy. Although transition metals based on Ni alloy catalysts can suppress the formation of carbon deposits over the pure Ni catalysts to some extent, this improvement significantly increases the cost and difficulty of synthesizing the catalysts.

Up until now, the influence of the SOFC anode environment on the underlying electrocatalytic mechanisms has remained largely uninvestigated. When a metal is brought in contact with a solid or liquid electrolyte, a common boundary (Stern layer)<sup>26</sup> between the two different phases results in a huge potential drop. The potential difference between electrode and electrolyte is about -3 to 3 V<sup>27-29</sup> and combines the effects of the electronic structure of the electrode, the adsorption species at the interface and the effective potential of the bulk solution. For the Stern layer, the thickness is about 2 Å to 8 Å.<sup>30</sup> As a result, the corresponding interfacial electric fields are in the range of  $\pm 0.375 \text{ V}/\text{Å}$  to  $\pm 1.5 \text{ V}/\text{Å}$ . This magnitude of electric fields can greatly influence the electronic orbitals of atoms or molecules and consequently affects the electrocatalytic reactions occurring near the electrode-electrolyte interface.<sup>23</sup> Experimentally, Sekine et al.<sup>31-33</sup> studied the electrocatalytic steam reforming of methane in the presence of an electric field. They found that in the presence of an electric field the conversion of methane over Pd/CeO<sub>2</sub>, Rh/CeO<sub>2</sub> and Pt/CeO<sub>2</sub> increased. In particular, they found that the conversion of methane occurred at 423 K with an external electric field, which is a temperature where a conventional catalytic reaction would hardly proceed.

We propose to examine the effects that this high electric field, in the order of -1 V/Å to 1 V/Å, has on the performance of the Ni-based anode. Quantum mechanical modeling methods based on DFT can be used to study the external electric field effect on the surface-adsorbate interactions that contribute to the surface structure and reactivity and ultimately control the overall electrocatalytic activity of the Ni anode. Stepped sites have more active centers for the nucleation of a graphene sheet, which can result in the formation of coke on a Ni surface.<sup>17</sup> From our previous work,<sup>34</sup> we established that a positive electric field suppresses the formation of

carbon on a Ni(111) surface because it significantly increases the energy barrier to form pure carbon deposits. In this work, external electric fields are applied to the methyl decomposition reaction on a stepped Ni(211) surface so as to see what are the effects of the step sites. The decomposition elementary reactions of methyl species are shown in Eq. (3), where  $x$  equals 1~3.



In this paper, we consider how an external electric field, in the order of 1.0 V/Å to -1.0 V/Å, can alter the decomposition of methyl species on a Ni(211) surface. This paper is organized as follows. The setup details of the DFT calculations are presented in Section 2. In Section 3, we present the results of the adsorption energies and the optimized geometries of the methyl species. The investigation of the co-adsorption energies of  $CH_x$  and H in the presence and absence of an external electric field will be carried out. A discussion of the external electric field effect on the transition state (TS) configurations, the energy barriers and reaction pathways of the elementary decomposition reaction of  $CH_x$  species on the Ni(211) surface will be given as well. Additionally, a comprehensive mechanistic picture overview of the  $CH_x$  species ( $x=1\sim 3$ ) on the Ni(211) surface with and without external electric fields will be given. Finally, the main findings and conclusions are summarized in Section 4. Throughout the results and discussion section, we will compare the electric field effects on a Ni(211) surface with those obtained on a Ni(111) surface in the presence of a field<sup>34</sup> and with the Au/Ni(211) surface in the absence of a field.<sup>20</sup>

## 2. Computational Methods

DFT calculations were performed using the Vienna *Ab Initio* Simulation package (VASP). To solve the Kohn-Sham equations,<sup>35</sup> the electronic structure calculations combined the projector-augmented wave (PAW)<sup>36</sup> method with the generalized gradient approximation (GGA),<sup>37, 38</sup> which is parameterized by the Perdew-Wang 91 (PW91)<sup>39</sup> functional. All the calculations were performed with spin-polarized electrons which accounts for the ferromagnetic nature of the Ni surface.<sup>40</sup> The quasi-Newton algorithm was adopted to relax the ions into their groundstate.<sup>41</sup> Geometries were considered optimized when the energy had converged to  $10^{-4}$  eV and the forces were smaller than 0.03 eV/Å. The plane-wave basis set was expanded to a kinetic energy maximum of 400 eV for the Kohn-Sham orbitals. The first-order Methfessel-Paxton smearing method<sup>8</sup> with a width of 0.1 eV was utilized to account for partial occupancies around the Fermi level and to speed up the convergence.

Here, the calculations will examine one of the simplest stepped surfaces of Ni, the (211) surface, as it has terrace sites and undercoordinated step-edge sites.<sup>4, 7</sup> For Ni(211), as shown in Fig. 1, a five-layer metal slab was modeled using a  $2 \times 4$  supercell<sup>20</sup> where the uppermost two

layers parallel to the step were fully relaxed while the remaining atoms were fixed at their bulk phase positions. In the calculations, each of the slabs was separated by approximately 12 Å of vacuum to ensure that the adsorbates and the subsequent slab would not interact. Such a vacuum layer is comparable to those used in the literature, where spacings ranging from 10 Å<sup>17,42</sup> to 12 Å<sup>20</sup> have been reported. The Brillouin zone was sampled by a  $5 \times 3 \times 1$  array of  $k$ -points with a Monkhorst-Pack grid.<sup>43</sup> The Ni lattice constant was theoretically calculated to be 3.521 Å from our previous work,<sup>34</sup> and is within 0.08% of the experimental value of 3.524 Å.<sup>44</sup>

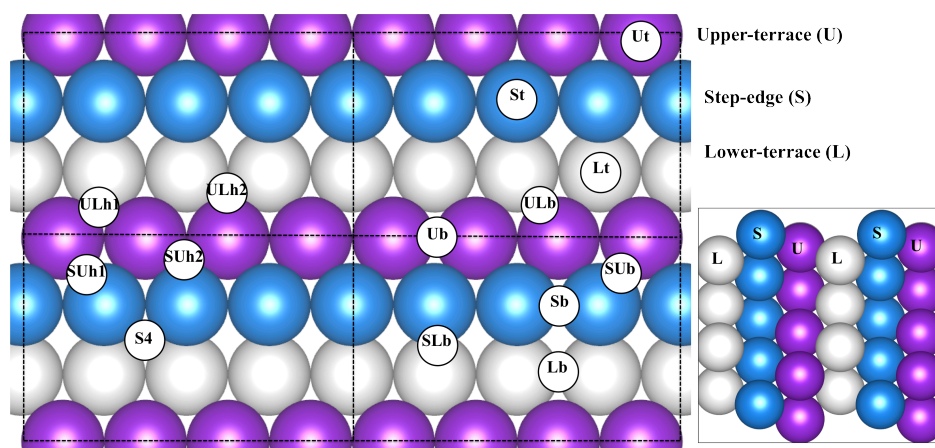


Fig. 1. Top and side views of a Ni (211) surface and the notation of adsorption sites. The details of the adsorption sites notation are explained in the first paragraph of Section 3.1.

The adsorption energy  $E_{\text{ads}}$  of methyl species on the Ni(211) surface was defined as follows:

$$E_{\text{ads}} = E_{(M/\text{slab})} - E_{(M)} - E_{(\text{slab})} \quad (4)$$

Where  $E_{(M/\text{slab})}$ ,  $E_{(M)}$  and  $E_{(\text{slab})}$  are the total energies of the slab with adsorbed species, isolated adsorbates in gas phase and the clean surfaces, respectively. The co-adsorption energy of A and B on Ni(211) with regards to the  $AB^* \rightarrow A^* + B^*$  reaction was calculated based on two different definitions: the separate reaction energy  $E_s$ , and co-adsorption reaction energy  $E_c$  given as follows:

$$E_s = (E_{(A/\text{slab})} + E_{(B/\text{slab})}) - (E_{(AB/\text{slab})} + E_{(\text{slab})}) \quad (5)$$

$$E_c = E_{((A+B)/\text{slab})} - E_{(AB/\text{slab})} \quad (6)$$

Where  $E_{(A/\text{slab})}$ , and  $E_{(B/\text{slab})}$ ,  $E_{(AB/\text{slab})}$  are the total energies of the adsorbates  $A^*$ ,  $B^*$  and  $AB^*$  on the Ni(211) surfaces, respectively.  $E_{((A+B)/\text{slab})}$  is the total energy of the co-adsorbed A and B species on a Ni(211) surface. Here  $E_s$  is used to define the thermal properties of reactions, where a

negative value means the reaction is exothermic while a positive value means the reaction is endothermic. The most stable co-adsorption configurations for calculating the minimum energy pathways have the weakest co-adsorption reaction energy  $E_c$ .

Both the nudged elastic band (NEB)<sup>45, 46</sup> and the climbing image nudged elastic band (CINEB)<sup>47</sup> methods were used to determine the minimum energy pathways for the decomposition of the  $\text{CH}_x$  species ( $x=1\sim 3$ ) at steps. The CINEB differs slightly from the NEB method since the highest image is moved towards the saddle point. The NEB method optimizes the images with an equal distance between the images, but the highest image may not be located exactly at the saddle point. It is better to optimize the images along the reaction pathway with the NEB method before using the CINEB method to obtain a good guess of the transition state because the highest energy image after optimizing with the NEB method is likely close to the saddle point. As a result, the CINEB method will be easier to converge after an initial run with the NEB method. If we only use the CINEB method to calculate the saddle point, the pathway would be difficult to converge with the poor initial guess of the interpolated images between the reactant and product. The transition states<sup>48</sup> were further verified by performing a vibrational frequency analysis to confirm a unique normal mode eigenvector corresponding to the negative curvature at the saddle point.<sup>9, 49</sup>

### 3. Results and Discussion

Table 1 summarizes the adsorption energies of all stable isolated  $\text{CH}_x$  ( $x=1\sim 3$ ) species on the Ni(211) surface. In combination with Table 1, the site preferences and the electric field effects on the adsorption energies and geometries of the  $\text{CH}_x$  species adsorbed on the Ni(211) surface are reported in the text. In addition, we will investigate the effects of the external electric fields on the elementary reactions involving the decomposition of methyl species on the Ni(211) surfaces, including the co-adsorption energies of  $\text{CH}_x$  and H species, the configurations along with the reaction pathways and decomposition energy barriers in the presence and absence of electric fields. Finally, a comparison of our results on Ni(211) with those obtained on Ni(111)<sup>34</sup> as well as with the similar work that was performed on an alloy Au/Ni(211) surface<sup>20</sup> will be made.

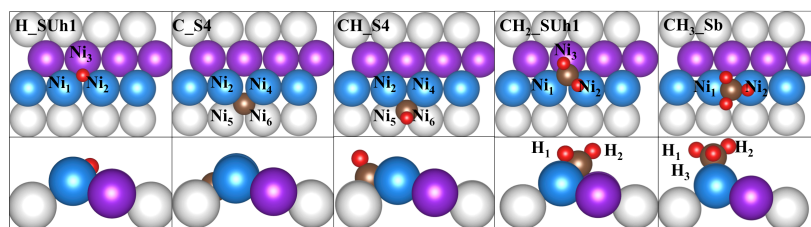


Fig. 2. Top and side views of optimized configurations for the most stable adsorption sites of (from left to right) H, CH, CH<sub>2</sub> and CH<sub>3</sub> on a Ni (211) surface. Only the topmost Ni (211) layer is shown and the notations of adsorption sites refer to Fig. 1. The red spheres represent hydrogen atoms while the brown spheres are carbon atoms.

### 3.1 Adsorption of H on the Ni(211) surface

As shown in Fig. 1, 14 different adsorption configurations of hydrogen atoms on Ni(211) were calculated. These were a hollow site (h) between the Step-edge and Upper-terrace (SUh1 and SUh2), a hollow site between the Upper and Lower-terrace (ULh1 and ULh2), a four-fold hollow site (S4), three top sites (t) including a Step-edge (St), Upper-terrace (Ut) and Lower terrace (Lt), six bridge sites (b) including the bridge sites between only Step-edge (Sb), Upper-terrace (Ub), Lower-terrace (Lb), Step-edge and Upper-terrace (Sub), Step-edge and Lower-terrace (SLb), Upper-terrace and Lower-terrace (ULb). Our calculations showed that 8 adsorption sites were stable for the single H atoms on the Ni(211) surface and the adsorption energies of these stable geometries are summarized in Table 1. For all of the other unstable adsorption sites of the H atoms except the Lt site, they shifted to their neighboring three-fold hollow site. For a H atom adsorbed at the Lt site, it shifted to the nearby SLb site. The most favorable adsorption structure for a H atom was the SUh1 site, with bond lengths of H-Ni<sub>1</sub>, H-Ni<sub>2</sub>, and H-Ni<sub>3</sub> being 1.694 Å, 1.695 Å and 1.747 Å (Fig. 2). The site preferences and structure characteristics are in good agreement with the results from Catapan et al.<sup>50</sup> (Table 1). Compared with our previous work<sup>34</sup> from the most stable site of a H atom on the Ni(111) surface, the adsorption energy of a H atom at its most stable site on Ni(211) was slightly stronger than that of the Ni(111) surface.

Additionally, we studied the electric field effect on a H atom adsorbed at the most stable site on the Ni(211) stepped surface, as shown in Fig. 3(a). After applying external electric fields, ranging from -1 V/Å to 1 V/Å, the electronic structures of the H atom slightly changed and the adsorption energy for the most favorable site fluctuated around 0.06 eV. More details of the electronic structures of the hydrogen or hydrocarbon species on Ni(211) is given in Electronic Supplemental Material Table 1S. When the electric field of -0.4 V/Å was applied, the H atom was seen to have the strongest adsorption energy. Both positive electric fields and negative electric fields slightly strengthened the adsorption energies of a single H atom on the Ni(211) surface. The electric field dependence of the adsorption energy can be parameterized as

$$E = E_0 + \vec{d} \cdot \vec{F} + \frac{\alpha}{2} F^2 \quad (7)$$

Where  $|\vec{d}|$  and  $\alpha$  can be regarded as an effective dipole moment and effective polarizability, respectively.<sup>51</sup> Our results showed that the value of the dipole moment of a single H atom on Ni(211) is two times larger than the estimated value of 0.01 eV·Å/V for a H atom on the Ni(111) surface,<sup>34</sup> which means a local electric field effect on a single H atom at this most favorable site on Ni(211) is stronger than that of the fcc site on Ni(111). Particularly, from Fig. 3(a), it is clear that the tendency of the electric field effects on a single H atom adsorbed on Ni(211) is larger than that of Ni(111) surface as shown by its higher degree of curvature. Table 2 summarizes the values of the effective dipole moment  $|\vec{d}|$  and the effective polarizability  $\alpha$  for the CH<sub>x</sub> species adsorbed on the Ni(211) surface.

**Table 1.** Summary of Adsorption Energies of Stable Hydrocarbon Species on Ni(211)

Species (Sites)	Eads (eV)	Species (Sites)	Eads (eV)
H (Sb)	-2.775	CH <sub>2</sub> (ULh2_1)	-3.891
H (SLb)	-2.622	CH <sub>2</sub> (ULh2_2)	-4.074
H (Lb)	-2.685	CH <sub>2</sub> (Sb_1)	-4.325
H (S4)	-2.698	CH <sub>2</sub> (S4_1)	-4.319
<b>H (SUh1)</b>	<b>-2.856</b> , -2.73 <sup>b</sup> , -2.89 <sup>c</sup>	CH <sub>2</sub> (S4_2)	-4.195
H (SUh2)	-2.791	CH <sub>2</sub> (SUh1_1)	-4.355, -4.47 <sup>a</sup>
H (ULh1)	-2.789	<b>CH<sub>2</sub> (SUh1_2)</b>	<b>-4.385</b>
H (ULh1)	-2.755	CH <sub>2</sub> (SUh2_1)	-4.222
<b>C (S4)</b>	<b>-7.976</b> , -7.96 <sup>a</sup> , -7.45 <sup>b</sup> , -7.85 <sup>c</sup>	CH <sub>2</sub> (SUh2_2)	-4.128
C (SUh1)	-7.074	CH <sub>3</sub> (SLb_3)	-1.704
C (SUh2)	-6.825	<b>CH<sub>3</sub> (Sb_2)</b>	<b>-2.369</b> , -2.59 <sup>a</sup> , -2.23 <sup>c</sup>
C (ULh1)	-6.805	CH <sub>3</sub> (SUh1_2)	-2.261
CH (SLb)	-5.724	CH <sub>3</sub> (SUh2_1)	-1.993
<b>CH (S4)</b>	<b>-6.869</b> , -6.70 <sup>a</sup> , -7.02 <sup>b</sup> , -6.79 <sup>c</sup>	CH <sub>3</sub> (LUh1_2)	-1.725
CH (SUh1)	-6.588	CH <sub>3</sub> (St_1)	-1.991
CH (SUh2)	-6.454	CH <sub>3</sub> (St_2)	-1.992
CH (ULh1)	-6.430	CH <sub>3</sub> (St_3)	-1.997
CH <sub>2</sub> (St_2)	-3.133	CH <sub>3</sub> (Ut_1)	-1.705
CH <sub>2</sub> (SLb_2)	-3.994		

<sup>a</sup> from Ref.<sup>20</sup>; <sup>b</sup> from Ref.<sup>50</sup>; <sup>c</sup> from Ref.<sup>52</sup>

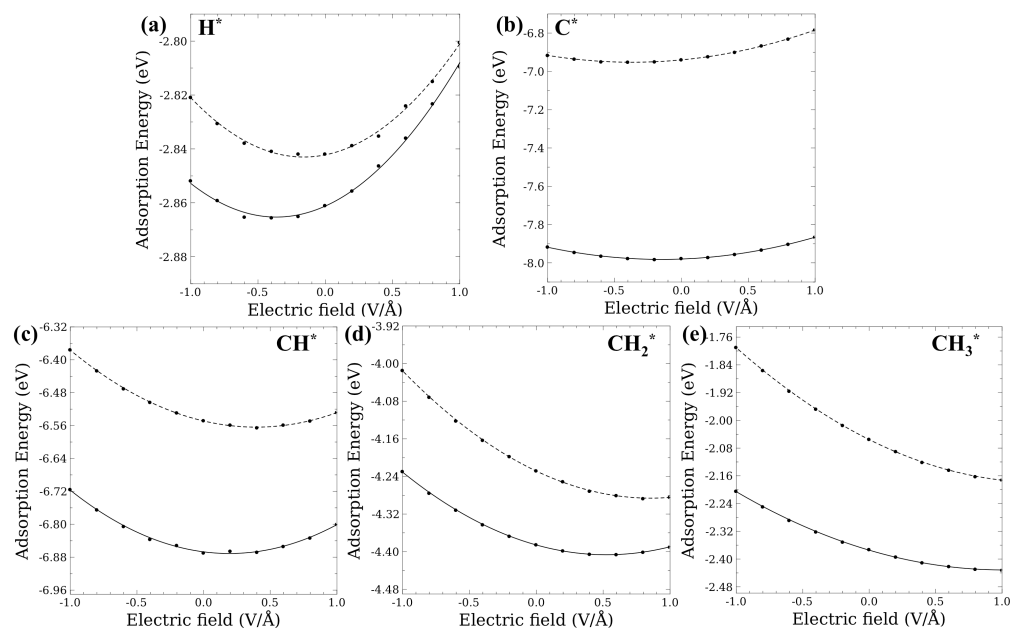


Fig. 3. The effect of an applied external electric field on the adsorption energies of various hydrocarbon species adsorbed on the Ni catalysts. Graphs (a), (b), (c), and (d) show the adsorption energy parabolic trend lines for H, C, CH, CH<sub>2</sub> and CH<sub>3</sub> species adsorbed on both the Ni (211) surface (continuous line) and the Ni (111) surface (dotted line), respectively.

### 3.2 Adsorption of hydrocarbon species on Ni(211)

#### 3.2.1 Adsorption of carbon on the Ni(211) surface

Comparing the eight stable adsorption sites of the H atoms on the Ni(211) surface, the results show that carbon atoms only had 4 stable adsorbed sites, including the S4, SUh1, SUh2, and ULh1 sites (the notations of adsorption sites are shown in Fig. 1) with the binding energies given in Table 1. For C atoms, the other unstable adsorption sites shifted to the adjacent three- or four fold hollow sites. From the results, the C atom prefers to bind at the four-fold hollow site (S4) on the Ni(211) surface with an adsorption energy of -7.967 eV, which is 1.028 eV stronger than that on the Ni(111) surface.<sup>34</sup> Therefore, C atoms are more strongly bonded on the stepped Ni(211) surface than the Ni(111) surface, verifying that C atoms are more easily adsorbed on the stepped surface as compared to the Ni(111) surface. The bond lengths of C-Ni<sub>2</sub>, C-Ni<sub>4</sub>, C-Ni<sub>5</sub>, C-Ni<sub>6</sub> are 1.821 Å, 1.822 Å, 1.846 Å and 1.846 Å, respectively (Fig. 2).

**Table 2.** Summary of the effective dipole moment ( $|\vec{d}|$ ) and the effective polarizability ( $\alpha$ ) values of hydrocarbon species on both the Ni(211) surface and the Ni(111) surface (in parenthesis)<sup>34</sup>

Species (Sites)	$\vec{d}$ (eV·Å/V)	$\alpha$ (Å <sup>2</sup> /V)	Species (Sites)	$\vec{d}$ (eV·Å/V)	$\alpha$ (Å <sup>2</sup> /V)
H (SUh1)	0.022 (0.010)	0.062 (0.062)	CH <sub>3</sub> (Sb_2)	-0.113 (-0.191)	0.112 (0.148)
C (S4)	0.026 (0.066)	0.176 (0.180)	CH <sub>2</sub> , H (Sb_1, SUh1)	0.103 (0.059)	0.011 (0.020)
CH (S4)	-0.042 (-0.076)	0.216 (0.193)	CH, H (S4, SUh1)	0.056 (0.063)	0.059 (0.009)
CH <sub>2</sub> (SUh1_2)	-0.079 (-0.135)	0.151 (0.157)	C, H (S4, SUh1)	0.089 (0.155)	0.018 (0.036)

An investigation of an external electric field effect on the most stable site for a C atom adsorbed on the Ni(211) surface was conducted. From Fig. 3(b), both positive and negative electric fields weakened the bonding strength of the C atoms, as it was the case for H on a Ni(211) surface. The C atoms adsorbed on Ni(211) reached the strongest adsorption energy of -7.983 eV when an external electric field of -0.2 V/Å was applied. The positive electric fields decreased the bond strength much more than negative field values. In the presence of a positive electric field of 1.0 V/Å, the C atom has its weakest adsorption energy of -7.866 eV. On the other hand when Huang et al.<sup>20</sup> added 1/4 ML Au onto the step-edge of a Ni(211) surface, they found that the adsorption energy of a C atom was weakened by 0.03 eV. This is a much smaller effect than what we report here in the presence of an external electric field. The calculated dipole moment is 0.026 eV·Å/V (Table 2) is slightly smaller than the dipole moment for a C atom adsorbed on a Ni(111) surface.<sup>34</sup> The parabolic fits to the electric field dependence of the adsorption energies for the C atoms on both Ni(211) and Ni(111) are almost parallel, suggesting that the influences of the electric fields on both systems are similar.

### 3.2.2 Adsorption of CH on the Ni(211) surface

The CH molecule adsorbed on the Ni(211) surface has five stable configurations, the SLb, S4, SUh1, SUh2 and ULh1 (Fig. 1), and the adsorption energies are summarized in Table 1. For all stable configurations, the C-H bond is vertical to the adsorption site. For the unstable structures, the Lt site for the CH molecule shifted to the nearby SLb site and the other unstable sites shifted to the adjacent stable three- or four- fold hollow sites. The four-fold hollow site (S4) is the most favorable one for a CH molecule adsorbed on the Ni(211) surface, with an adsorption energy of -6.869 eV, a C-H bond length of 1.109 Å and C-Ni<sub>2</sub>, C-Ni<sub>4</sub>, C-Ni<sub>5</sub> and C-Ni<sub>6</sub> bond lengths of 1.940 Å, 1.941 Å, 1.947 Å, and 1.947 Å, respectively (see Fig. 2). We also note that

the H-C-Ni<sub>2</sub>, H-C-Ni<sub>4</sub>, H-C-Ni<sub>5</sub> and H-C-Ni<sub>6</sub> angles are 114.1°, 114.0°, 120.3° and 120.3°, respectively. In addition, the adsorption energy at this site is 0.321 eV stronger than the adsorption of a CH molecule at the most favorable fcc site on a Ni(111) surface.<sup>34</sup> Comparing the adsorption energy of CH at the most favorable S4 site with the literature, our results are in good agreement with those from Huang et al.,<sup>20</sup> Rafael et al.<sup>50</sup> and Zhao et al.<sup>53</sup>.

A significant difference was seen from the trend lines of the electric field effects on the adsorption energies of the H and C species. The positive electric field effects on the adsorption energies of the CH molecules are much weaker than the negative ones. The magnitude of the adsorption energy of a CH molecule weakened to its minimum value of -6.715 eV at an external electric field of -1.0 V/Å. The adsorption energy was strongest on the stepped surface when no electric field was applied. The calculated values of  $|\vec{d}|$  and  $\alpha$  (Table 2) confirms that a negative electric field decreases the stabilities of CH species on a Ni(211) surface. The value of  $|\vec{d}|$  for the CH species adsorbed on Ni(111) is -0.076 eV·Å/V,<sup>34</sup> which is 0.034 eV·Å/V more negative than the dipole moment of the Ni(211) surface. Therefore, the effect of the external electric field on the adsorption energies of the CH species on Ni(111) is much stronger than that on Ni(211).

### 3.2.3 Adsorption of CH<sub>2</sub> on the Ni(211) surface

We examined the same fourteen-adsorption sites for the adsorption of CH<sub>2</sub> on Ni(211) as we did for the H, C and CH groups, but for each site two or three possible orientations were considered, as shown in Fig. 4. With regard to these thirty-one structures for the CH<sub>2</sub> species adsorbed on the Ni(211) surface, eleven stable adsorption configurations were found to be stable, including one top site (St\_2), two bridge sites (SLb\_2, Sb\_1), three three-fold hollow sites with two orientations (SUh1\_1, SUh1\_2, SUh2\_1, SUh2\_2, ULh2\_1 and ULh2\_2) and a four-fold hollow site with two orientations (S4\_1, S4\_2). From the results shown in Table 1, it is clear that the most stable configuration is the SUh1\_2 site (Fig. 2), with an adsorption energy of -4.385 eV, which is only 0.03 eV stronger than that of the same adsorption site but with a different orientation (SUh1\_1). The adsorption energy for this SUh1\_2 configuration was found to be slightly stronger than a CH<sub>2</sub> molecule adsorbed at the fcc site on Ni(111). It is also worth mentioning that the CH<sub>2</sub> species themselves are only symmetric at the stable top and bridge sites, with a C-H bond length of 1.10 Å. For the CH<sub>2</sub> molecules adsorbed at the three- or four-fold hollow sites on Ni(211), the adsorbates are not symmetric, where the longer C-H bond length is 1.23 Å and the shorter C-H bond length is 1.10 Å. All the stable hollow sites have much stronger adsorption energies than the top and bridge sites (Table 1).

An external electric field, ranging from  $1.0 \text{ V/\AA}$  to  $-1.0 \text{ V/\AA}$ , was applied onto the most stable SUh1\_2 site of the  $\text{CH}_2$  molecule adsorbed on the Ni(211) surface, as shown in Fig. 3(d). The trend line was the same as for the CH molecule on the Ni(211) surface, with a dipole moment of  $-0.079 \text{ eV}\cdot\text{\AA}/\text{V}$  (Table 2). By adding a large negative electric field of  $-1.0 \text{ V/\AA}$ , the magnitude of the adsorption energy monotonically weakened to  $-4.229 \text{ eV}$ . When an electric field of  $0.6 \text{ V/\AA}$  was applied, the magnitude of the adsorption energy of the  $\text{CH}_2$  group reached its maximum value of  $-4.406 \text{ eV}$ . The electric field effect is again smaller on the Ni(211) surface than that on the Ni(111) surface.<sup>34</sup> In addition, for the most stable adsorption structure for  $\text{CH}_2$  on Ni(211), the bond lengths between the C atom and the bonded Ni atoms significantly decreased after applying a positive electric field, leading to a stronger interaction between the adsorbate and the Ni surface and a stronger adsorption energy of the  $\text{CH}_2$  molecule as compared with the scenario without an electric field. On the other hand, when we applied a positive electric field, the C-Ni bond lengths increased, which resulted in a weaker adsorption energy of the  $\text{CH}_2$  molecule.

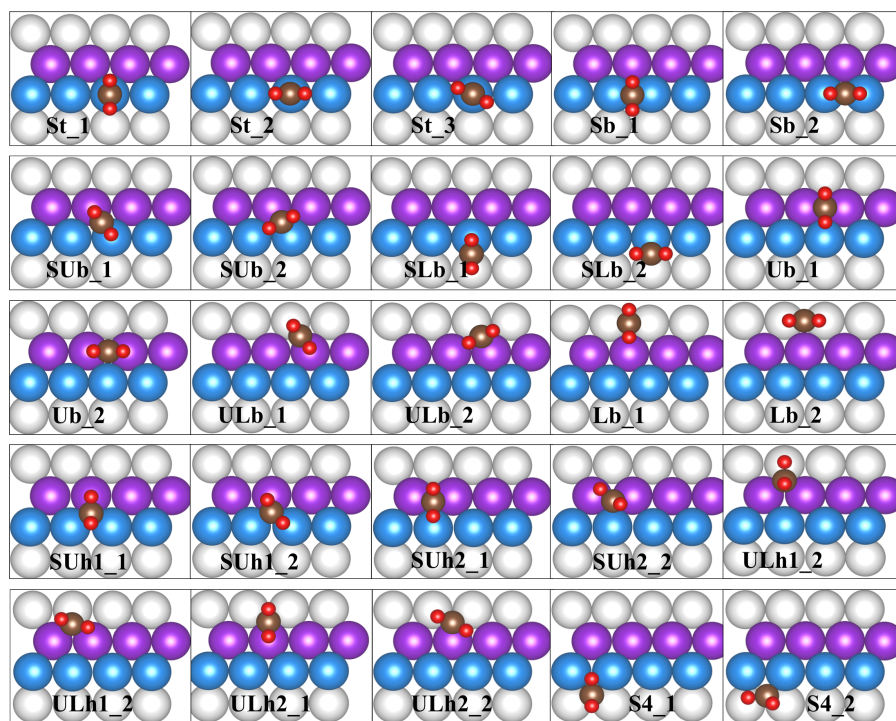


Fig. 4. Configurations considered for the adsorption of the  $\text{CH}_2$  species on the Ni (211) surface. Only the topmost Ni (211) layer is shown and the notations of adsorption sites refer to Fig. 1. For the adsorption of the  $\text{CH}_2$  molecules on Ni (211), we examined the same H orientations of the top sites on the Upper-terrace (not shown) and Lower-terrace atoms (not shown) that were considered on the top of the step-edge atoms (St\_1, St\_2 and St\_3), but we didn't show their configurations here.

### 3.2.4 Adsorption of $\text{CH}_3$ on the Ni(211) surface

Compared to the initial configurations of the H, C, CH and  $\text{CH}_2$  species on Ni(211), the  $\text{CH}_3$  group showed more variation at each adsorption site (Fig. 6). After the optimization of each of these configurations, only nine structures were stable; two top sites with different orientations, the top sites of the Step-edge (St\_1, St\_2, St\_3) and the top site of Upper-terrace (Ut\_1), two bridge sites (SLb\_3 and Sb\_2), and three-fold hollow sites (SUh1\_2, SUh2\_1 and LUh1\_2). The  $\text{CH}_3$  molecule adsorbed at the bridge site (Sb\_2) between two Step-edge surface atoms has the most favorable adsorption energy of -2.369 eV, which is in agreement with the literature (Table 1).<sup>20, 50, 52</sup> For this most favorable configuration, a H atom of the  $\text{CH}_3$  molecule sits at the top of the step-edge surface atom, with the Ni-H bond length of 1.808 Å and a C-H bond length of 1.143 Å (Fig. 2). The adsorption energy of this configuration is only 0.108 eV stronger than the SUh1\_2 site, but much stronger than the other stable sites. Additionally, the three orientations of the structures of St sites have almost the same adsorption energy of -1.99 eV.

An external electric field was applied on the most favorable site (Sb\_2) of a  $\text{CH}_3$  molecule on Ni(211) (Fig. 3(e)) as well. Comparing the results of the adsorption energies with different applied electric fields, it is clear that the adsorption energy of this system decreased monotonically from -2.204 at -1.0 V/Å to -2.432 eV at 1.0 V/Å. By examining the bond lengths of the  $\text{CH}_3$  molecule on the Ni(211) surface, we found that the C-Ni<sub>1</sub> and C-Ni<sub>2</sub> bond lengths increased from 1.990 Å and 2.066 Å to 1.997 Å and 2.095 Å at a field value of -1.0 V/Å. As a result, the adsorption energy of the  $\text{CH}_3$  molecule is weaker than the one without an electric field. Other bonds lengths are given in Table 1S in the Electronic Supplementary Material. The trend line of the electric field effect on this system is also similar to that of a  $\text{CH}_3$  molecule on a Ni(111) surface with a dipole moment of -0.113 eV·Å/V, which is slightly smaller than the Ni(111) surface.<sup>34</sup> These results suggest that the electric field effect on the  $\text{CH}_3$  adsorbate is similar between the two surfaces. In addition, we also examined the density of states (DOS) of the adsorbates on both the Ni(111) and Ni(211) surfaces in the presence and absence of electric fields. Because the differences between the spin up states and spin down states of C<sub>2p</sub> and H<sub>1s</sub> orbital are negligible we only present here the spin up states for the adsorbed  $\text{CH}_3$  molecule at its most favorable sites on both the Ni(111) and Ni(211) surfaces. The calculation results show that the peaks below the Fermi level of the C<sub>2p</sub> and H<sub>1s</sub> orbital shifted closer to the Fermi energy when we applied a positive electric field. As a result, the C<sub>2p</sub> and H<sub>1s</sub> orbital have more interaction with the d orbitals of the bonded Ni atoms, leading to a greater adsorption energy than when such a field is absent. On the other hand, when we applied a negative electric field, the peaks of the C<sub>2p</sub>

and  $H_{1s}$  orbital shift away from the Fermi energy, indicating less interaction between the  $C_{2p}$ ,  $H_{1s}$  orbitals and the d orbitals of the bonded Ni atoms resulting in a weaker adsorption energy. Such field effects on the  $CH_3$  molecule were much larger than on the corresponding Ni atoms. Indeed, we found that the effect of an external electric field on d band of the Ni atoms was a negligible. A more detailed discussion of these field effects on the density of states is given in the Electronic Supplementary Material.

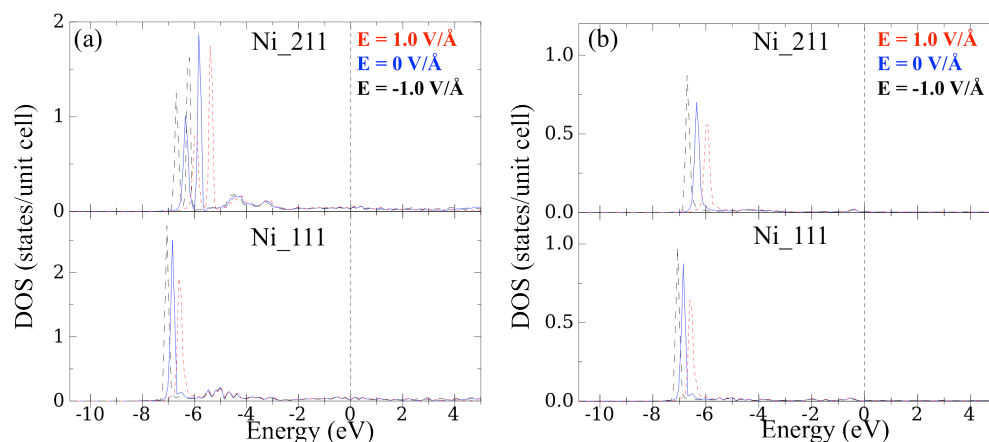


Fig. 5. The density of states projected of the (a)  $C_{2p}$  and (b)  $H_{1s}$  orbitals for the adsorbed  $CH_3$  molecule at the most stable site with and without electric fields. The energies refer to the Fermi energy, indicated by the vertical black dotted line.

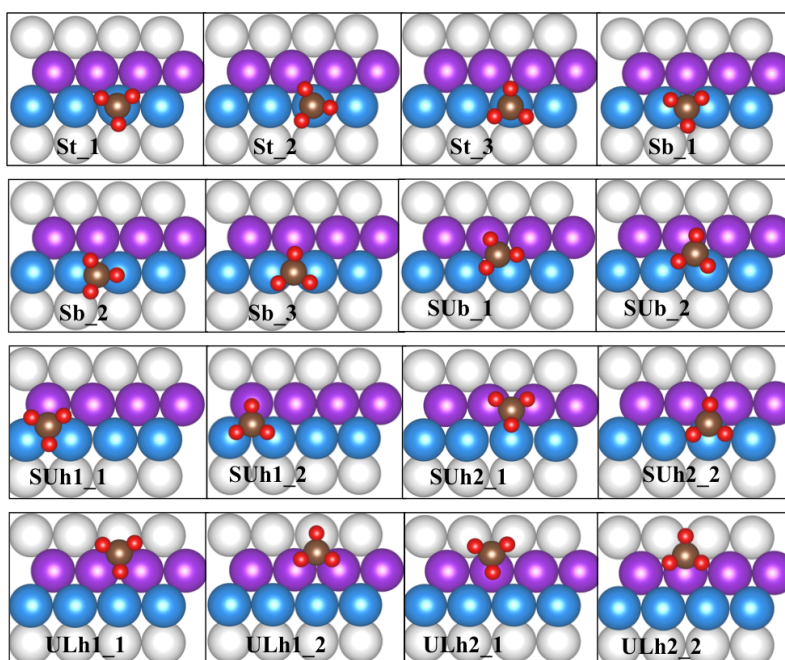


Fig. 6. Initial configurations for the CH<sub>3</sub> molecules adsorbed on Ni (211) with regard to fourteen different adsorption sites with two or three possible variations per site. Since the possible orientations of the CH<sub>3</sub> molecules bonding at the top sites of the Upper-terrace (Ut), the top sites of the Lower-terrace atoms (Lt) and the four-fold hollow site (S4) are the same as the top sites of Step-edge (St<sub>1</sub>, St<sub>2</sub> and St<sub>3</sub>), we did not show their structures here. Additionally, the possible orientations of the CH<sub>3</sub> species adsorbed at the SLb, Ub, Lb sites (not shown) are the same as at the Sb sites (Sb<sub>1</sub>, Sb<sub>2</sub> and Sb<sub>3</sub>). We also remark that the ULb sites (not shown) have the same possible orientations of CH<sub>3</sub> as shown for the SUB sites (SUB<sub>1</sub> and SUB<sub>2</sub>).

From the results comparison between Ni(211) stepped surfaces and Ni(111) flat surfaces, only the case of a H atom sitting at the three-fold hollow site between the Step-edge and Upper-terrace surface atoms (SUh1) on Ni(211) had a larger dipole moment than the one of a H atom adsorbed on the Ni(111) surface.<sup>34</sup> The CH<sub>x</sub> species at different adsorption sites had smaller effective dipole moments on the stepped Ni(211) surface. Based on this result, we assumed that the influence of an overall external electric field will significantly affect the local electric fields at different adsorption sites on the Ni(211) stepped surface. Therefore, the adsorption energies of all the stable sites of the CH<sub>3</sub> group in the presence and absence of an external electric field were studied (Fig. 7). When fitting these data to the parabolic equation, the order of the magnitudes of the dipole moments is given by: SUh2<sub>1</sub> > SUh1<sub>2</sub> > ULh1<sub>2</sub> > Sb<sub>2</sub> > SLb<sub>3</sub> > St<sub>3</sub>. This means that the local electric field has the largest effect on the SUh2 site and the smallest effect on the St site, which can be also seen from the slope of these curves in Fig. 7. When the electric field was varied from -1.0 V/Å to 1.0 V/Å, we calculated the changes in local electric field ( $\Delta F$ ) at different adsorption sites with respect to the local electric field value in the absence of such external fields.<sup>54</sup> The results showed that the SUh2<sub>1</sub> adsorption site has the largest change in local electric field  $\Delta F$ , in the range of -6.17 ~ 2.77 V/Å, which correlates well with its dipole moment value. In other words, when we applied -1.0 V/Å,  $\Delta F$  at the SUh2<sub>1</sub> site was shown to be of the order of -6.17 V/Å, while  $\Delta F$  was 2.77 V/Å when we applied a field of 1.0 V/Å. For the other adsorption sites,  $\Delta F$  ranges from -3.35 ~ 0.99 V/Å, -0.63 ~ 0.05 V/Å, -0.64 ~ 0.41 V/Å, -1.20 ~ 1.68 V/Å, -0.13 ~ 0.40 V/Å, for the SUh1<sub>2</sub>, ULh1<sub>2</sub>, Sb<sub>2</sub>, SLb<sub>3</sub>, St<sub>3</sub> sites, respectively, which is similar to the order as the magnitudes of their dipole moments. From Fig. 7, the external electric fields not only had different influences on the adsorption energies of different adsorption sites, but also changed the site preferences for the CH<sub>3</sub> species on Ni(211).

Fig. 8 shows the changes in local electric field distribution  $\Delta F$  as a function of Z (the coordinates along z-direction in supercell) at the different adsorption sites (SUh2<sub>1</sub>, Sb<sub>2</sub> and

St\_3) for the CH<sub>3</sub> group on the Ni(211) surface when an external electric field, in the range of 1 V/Å to -1 V/Å, is applied. As expected, a  $\Delta F$  value of 1 V/Å and -1 V/Å is obtained in the vacuum area from Fig. 8 ( $Z \geq 12.0$  Å). We also only plotted the changes in the local electric field distribution along the Z direction while the X and Y were fixed for the various positions of the different adsorption sites. The ranges of  $\Delta F$  as reported above were based on the local electric field differences at the Z position of the C atoms. In Fig. 8(c), the ranges of  $\Delta F$  are bigger than the other adsorption sites (Fig. 8(a) and 8(b)), suggesting that the C atom at the SUh2\_1 sites have larger changes in the local electric field range than for the C atoms sitting at the St\_3 and Sb\_2 sites. Particularly, when the carbon atom adsorbed at the St\_3 site (Fig. 8(a)), the ranges of  $\Delta F$  at the carbon atom Z position is the smallest. This again verifies the assumption that the different adsorption sites at the stepped Ni(211) surface have different magnitudes of  $\Delta F$ . However, even though the applied electric field on this SUh2 site on the Ni(211) surface has the most significant effect, it is still slightly smaller than that of the Ni(111) surface.<sup>34</sup>

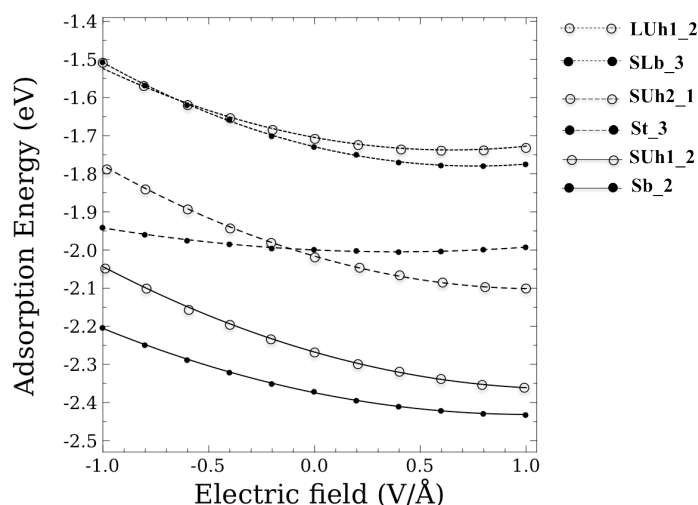


Fig. 7. The electric field effects on the adsorption energies of the CH<sub>3</sub> group at different adsorption sites on the Ni (211) surfaces. Different adsorption sites utilize different line types combined with different point styles (e.g. the continuous line with solid points represents the electric field effects on a CH<sub>3</sub> molecule sitting at the Sb\_2 site).

Overall, the adsorption energies of hydrocarbon species on the Ni(211) surface are stronger than those on the Ni(111) surface. For the isolated H and C atoms at their most favorable adsorption sites on the Ni(211) surface, the trend lines of the electric field effects are similar, where the positive electric fields weaken the adsorption energies of the adsorbates much more than the negative ones. On the other hand, for the isolated CH, CH<sub>2</sub> and CH<sub>3</sub> species at their most

stable sites on the Ni(211) surface, the negative electric fields weakened the adsorption energies of the isolated adsorbates much more than the positive ones. Particularly for the CH<sub>2</sub> and CH<sub>3</sub> groups, the adsorption energies are monotonically strengthened when the electric field is increased from -1.0 V/Å to 1.0 V/Å. However, except for the case of a H atom sitting at the SUh1 site on Ni(211) which has a larger dipole moment than the one on Ni(111), the other CH<sub>x</sub> species has smaller dipole moments on Ni(211) relative to Ni(111).<sup>34</sup> This indicates that the electric field effects on the adsorption energies of the CH<sub>x</sub> species are smaller on the stepped Ni(211) surface than on Ni(111). In addition, by examining the interactions of the CH<sub>3</sub> species with an external electric field at different adsorption sites on the Ni(211) surfaces, we found that different sites had different magnitudes of the local electric field differences.

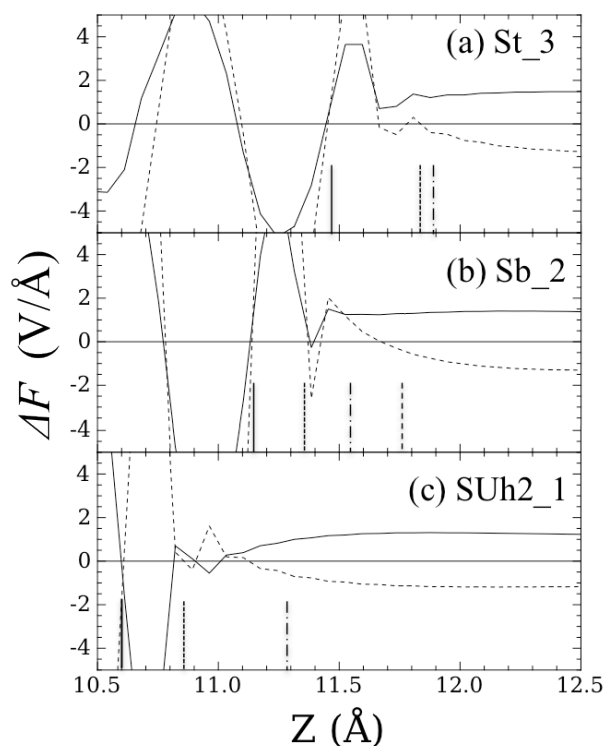


Fig. 8. The changes in the local electric field distribution  $\Delta F$  at the different adsorption sites of the CH<sub>3</sub> molecules on Ni(211) with respect to the local electric field value in the absence of such external fields. The  $\Delta F$  values are shown in the presence a positive electric field (continuous line), a negative electric field (short dashed line) by the comparison with the one without electric fields. Fig. 8(a), (b) and (c) shows the CH<sub>3</sub> molecule adsorption at St<sub>3</sub>, Sb<sub>2</sub> and SUh<sub>2\_1</sub> sites, respectively. The position of the C atoms on the surface are marked as solid vertical lines. For the positions of H atoms, (a) Two H atoms have the same Z position are shown as the vertical short-dash line and the long-dash-dotted line at the greater Z value represents the

third H atom; (b) The H atom on the top of the Step-edge atom are marked as short-dash line while the other two H atoms near the four- and three-fold hollow sites are shown as a vertical long-dash-dotted line and long-dash line, respectively; (c) the vertical short-dash line shows the H atom near the Step-edge and the vertical long-dash-dotted line at greater Z value represents the two other H atoms near the Upper-terrace because of their same height in the cell.

### 3.3 Co-adsorption of $CH_x$ species and a H atom on a Ni(211) surface

The initial images for each pathway for the methyl species decomposition reaction are identified from the previous results of the isolated hydrocarbon species on the Ni(211) surface. The next step is to investigate the most favorable co-adsorption sites for hydrocarbon species and a H atom co-adsorbed on the Ni(211) surface. Additionally, we will also report the calculations regarding the electric field effects on the decomposition reaction pathways of the methyl species on the Ni(211) surface and compare them to our previous work on the Ni(111) surface.<sup>34</sup>

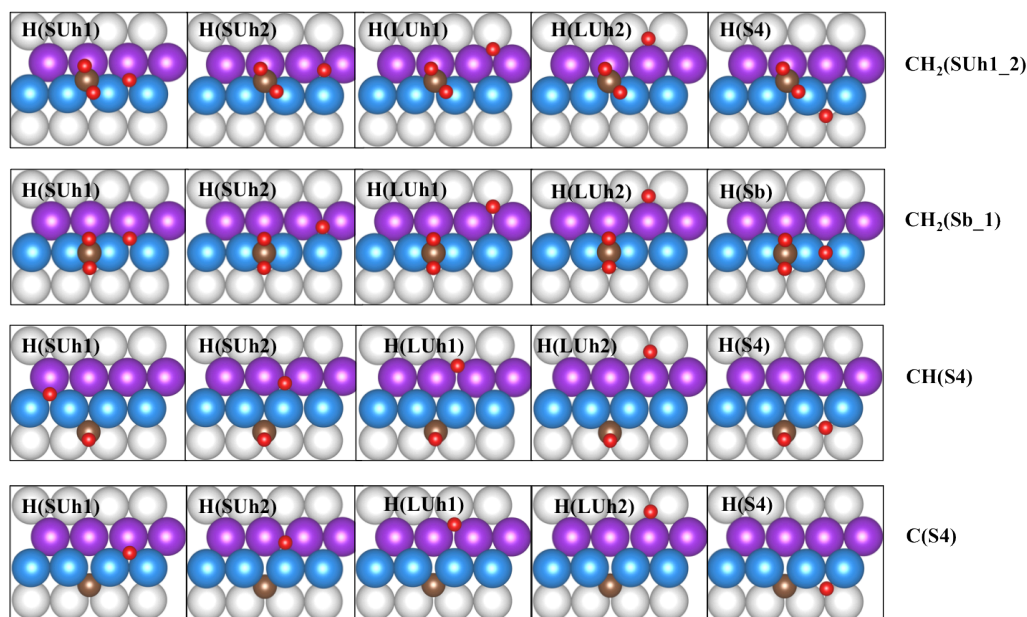


Fig. 9. The configurations considered for the different co-adsorption sites for the  $CH_x$  and H species on the Ni (211) surface.

#### 3.3.1 $CH_2$ and H co-adsorbed on a Ni(211) surface

The first co-adsorption system had a  $CH_2$  species and a H atom co-adsorbed on the Ni(211) surface. The initial configurations are shown in Fig. 9. Since the  $CH_2$  molecule at the SUh1\_2 site had the most favorable adsorption energy, we only investigated its position at the SUh1\_2 site in the configurations shown in the first row of Fig. 9 and co-adsorbed a H atom at

different adsorption sites. Another scenario was also considered, where a CH<sub>2</sub> molecule would adsorb at the Sb\_1 site, because the adsorption energy difference between the SUh1\_2 site and the Sb\_1 site on the Ni(211) surface was only 0.06 eV (configurations are shown in the second row in Fig. 9). From the results in Table 3, it is clear that the most favorable co-adsorption site for this system is the CH<sub>2</sub> molecule at the Sb\_1 site and a H atom at the nearby SUh1 site with a co-adsorption reaction energy of 0.243 eV, a bond length between the C atom and the co-adsorbed H atom of 2.811 Å, and C-H bond lengths in the CH<sub>2</sub> molecule of 1.098 Å and 1.104 Å. This configuration was used as the final image for the reaction pathway involving the decomposition of a CH<sub>3</sub> molecule to form a CH<sub>2</sub> molecule and a H atom. With regards to all configurations of the CH<sub>2</sub> and H species co-adsorbed on Ni(211), their separate reaction energies are all positive (Table 3), indicating that the  $CH_3^* \rightarrow CH_2^* + H^*$  reaction is endothermic.

In addition, an external electric field was applied to this co-adsorption system. The geometries of the structures did not significantly change. For the co-adsorption reaction energy, it monotonically increased from 0.145 eV at -1.0 V/Å to 0.352 eV at 1.0 V/Å (Fig. 10(a)). The dipole moment for this system is 0.103 eV·Å/V, which is given in Table 2. Comparing these results of the CH<sub>2</sub> and H species co-adsorption on the Ni(211) surface with the Ni(111) surface, the effective dipole moment on the Ni(211) system is almost two times larger than that of the Ni(111) surface,<sup>34</sup> suggesting that the electric field effect on a CH<sub>3</sub> molecule decomposition to form CH<sub>2</sub> and H species on the Ni(211) surface is more significant than that on the Ni(111) surface. Since the co-adsorption reaction energy of the CH<sub>2</sub> and H species on the Ni(111) surface ranges from 0.015 eV to 0.133 eV when electric fields of -1.0 V/Å to 1.0 V/Å were applied (Fig. 10(a)), the  $CH_3^* \rightarrow CH_2^* + H^*$  reaction is more endothermic on the Ni(211) surface than on the Ni(111) surface.

**Table 3.** Summary of the Co-adsorption Reaction Energy ( $E_c$  calculated by Eq. (6)) and Separate Reaction Energy ( $E_s$  calculated by Eq. (5)) of the CH<sub>x</sub> Species Co-adsorbed with a H atom.

Species (Sites)	$E_c$ (eV)	$E_s$ (eV)	Species (Sites)	$E_c$ (eV)	$E_s$ (eV)
CH <sub>2</sub> , H (SUh1_2, SUh1)	0.289	0.188	<b>CH, H (S4, SUh1)</b>	<b>-0.619</b>	<b>-0.541</b>
CH <sub>2</sub> , H (SUh1_2, SUh2)	0.273	0.260	CH, H (S4, SUh2)	-0.569	-0.473
CH <sub>2</sub> , H (SUh1_2, LUh1)	0.259	0.256	CH, H (S4, LUh1)	-0.259	-0.469
CH <sub>2</sub> , H (SUh1_2, LUh2)	0.308	0.292	CH, H (S4, LUh2)	-0.380	-0.437
CH <sub>2</sub> , H (SUh1_2, S4)	0.292	0.350	CH, H (S4, S4)	-0.312	-0.379
<b>CH<sub>2</sub>, H (Sb_1, SUh1)</b>	<b>0.243</b>	<b>0.249</b>	<b>C, H (S4, SUh1)</b>	<b>-0.378</b>	<b>-0.267</b>

CH <sub>2</sub> , H (Sb_1, SUh2)	0.311	0.318	C, H (S4, SUh2)	-0.284	-0.198
CH <sub>2</sub> , H (Sb_1, LUh1)	0.314	0.321	C, H (S4, LUh1)	-0.081	-0.195
CH <sub>2</sub> , H (Sb_1, LUh2)	0.348	0.354	C, H (S4, LUh2)	-0.125	-0.162
CH <sub>2</sub> , H (Sb_1, Sb)	0.302	0.333	C, H (S4, S4)	-0.071	-0.104

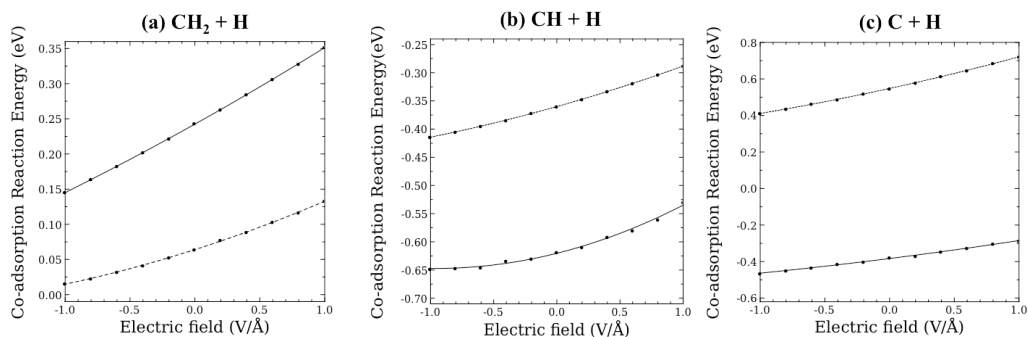


Fig. 10. The external electric field effect on the co-adsorption reaction energies of the most favorable configurations involving a CH<sub>x</sub> and H species on the Ni (211) surface (continuous line) with comparison of the Ni (111) surface (dotted line).

### 3.3.2 CH and H co-adsorbed on a Ni(211) surface

The third row in Fig. 9 shows the considered configurations for the CH and H species co-adsorption on the Ni(211) surface. Since the adsorption energy of the isolated CH molecule at the four-fold hollow site is much stronger than the other adsorption sites, calculations only considered the situation where the CH molecules sit at the S4 site co-adsorbed with a H atom at the different adsorption sites. The most favorable site for this system was the CH molecule at the S4 site with a H atom at the SUh1 site, with the co-adsorption reaction energy ( $E_c$ ) of -0.619 eV. The  $E_c$  of the other configurations are given in Table 3. This most stable structure contains a bond length between the C atom and the co-adsorbed H atom of 3.524 Å, a C-H bond length in the CH molecule of 1.109 Å. Different from the previous co-adsorption case of the CH<sub>2</sub> and H species, the separate reaction energies of these configurations are all negative, meaning that the reaction of  $CH_2^* \rightarrow CH^* + H^*$  is exothermic on Ni(211). As the electric field was applied, the trend line of the external electric field effects on this system is the same as the CH<sub>2</sub> and H species co-adsorption system. The  $E_c$  monotonically weakened to -0.530 eV at a field value of 1.0 V/Å and strengthened to a maximum of -0.648 eV at a field value of -1.0 V/Å. The calculated dipole moment was 0.056 eV·Å/V, verifying that an applied external positive electric field weakens the  $E_c$  of the CH and H species. From Fig. 10 (b), it is clear that the  $E_c$  of the CH and H species co-

sitting on the Ni(211) surface with and without the electric fields is much more negative than on the Ni(111) surface,<sup>1</sup> indicating that the  $CH_2^* \rightarrow CH^* + H^*$  reaction on the Ni(211) surface is more exothermic than on the Ni(111) surface.

### 3.3.3 C and H co-adsorbed on a Ni(211) surface

The last co-adsorption calculation step is the system of a C atom with a H atom on a Ni(211) surface. Because the C atoms at the four-fold hollow site (S4) are much more stable than the other adsorption sites, only one scenario is considered, where a C atom is adsorbed at an S4 site with a H atom adsorbed at different neighboring stable sites (initial configurations as shown in the last row in Fig. 9). From the results in Table 3, the structure of the C atom sitting at the S4 site with the co-adsorption of a H atom at the SUh1 site had the most favorable co-adsorption reaction energy, with an  $E_c$  of -0.378 eV. The separate reaction energies ( $E_s$ ) of all the considered co-adsorption configurations of C and H species are all negative, meaning that the reaction of  $CH^* \rightarrow C^* + H^*$  is exothermic. This result is significantly different to the Ni(111) surface<sup>34</sup> where this step is the most endothermic reaction of all the three-steps involved in the  $CH_3$  decomposition to pure carbon and hydrogen. This suggests that the CH molecules could spontaneously form pure C atoms on the Ni(211) surface, and finally result in the formation of coke on the Ni(211) surface, which verifies that carbon deposits are much easier to form on the stepped surface than on the close packed surface.<sup>17, 34</sup>

In addition to the above work, an investigation of an external electric field effect on this system was undertaken (Fig. 10(c)). The  $CH^* \rightarrow C^* + H^*$  reaction was found to proceed much more easily by applying the negative electric field of -1.0 V/Å, with a co-adsorption reaction energy of -0.464 eV. On the other hand, when a positive electric field of 1.0 V/Å was applied, the co-adsorption reaction energy increased to -0.286 eV. The dipole moment of the C and H species co-adsorbed on Ni(211) is still smaller than that on Ni(111) (Table 2).

## 3.4 Transition State and Energy Barriers

### 3.4.1 Reaction Pathway: $CH_3^*(Sb\_2) \rightarrow CH_2^*(Sb\_1) + H^*(Sb) \rightarrow CH_2^*(Sb\_1) + H^*(SUh1)$

Fig. 11 shows that the reaction pathway of a  $CH_3$  molecule at the most favorable Sb\_2 site, undergoing dissociation into a  $CH_2$  molecule at the Sb\_1 site with a H atom at the SUh1 site, which goes through an intermediate minimum (as shown in Fig. 11C). In order to address this issue, we used the same method as the previous work done on the Ni(111) surface,<sup>34</sup> separating this pathway into two parts for consideration. The H atom abstraction from a  $CH_3$  molecule

initiates with the C-H bond tilting toward to the step-edge. Initially, the C-H bond length is 1.143 Å, where the active H atom is along the step-edge. At the TS, the leaving H atom adsorbed at the St site has a C-H bond length of 1.788 Å, well over the C-H bond length in a CH<sub>3</sub> molecule, suggesting that the C-H bond had been broken at the TS. The active H atom moved to the Sb site with a CH<sub>2</sub> molecule remaining at the original Sb site to form the intermediate, with a C-H bond length of 2.584 Å. In the second part of this pathway, the H atom shifted from the Sb site to the SUh1 site, with a final C-H bond length of 2.811 Å. During the first part of the pathway, the energy barrier of  $CH_3^*(Sb\_2) \rightarrow CH_2^*(Sb\_1) + H^*(Sb)$  was found to be 0.627 eV (as shown in Table 4), which is slightly smaller than the one on the Ni(111) surface. The first part of the pathway leads to a product lying 0.302 eV in energy above the reactants. In the second part pathway of  $CH_2^*(Sb\_1) + H^*(Sb) \rightarrow CH_2^*(Sb\_1) + H^*(SUh1)$ , the product lowers the reaction energy by -0.059 eV.

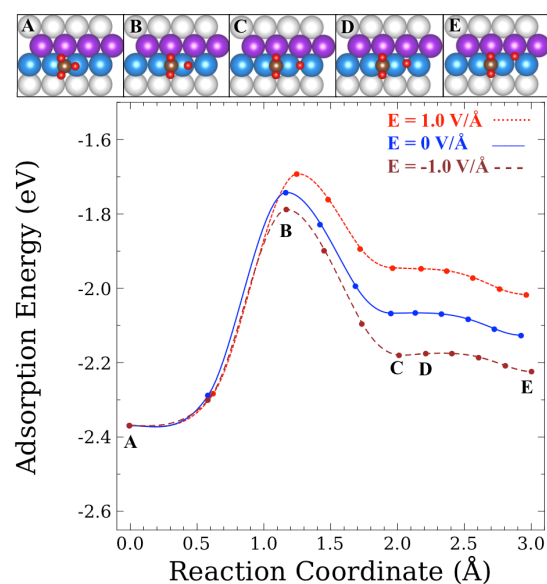


Fig. 11. The  $CH_3^*(Sb\_2) \rightarrow CH_2^*(Sb\_1) + H^*(Sb) \rightarrow CH_2^*(Sb\_1) + H^*(SUh1)$  reaction minimum energy pathway with and without an external electric field. The A-E images show the structure configurations along with this pathway.

By adding a positive electric field of 1.0 V/Å, the energy barrier of the first part of the pathway ( $CH_3^*(Sb\_2) \rightarrow CH_2^*(Sb\_1) + H^*(Sb)$ ) increased to 0.677 eV. On the other hand, the energy barrier decreased to 0.581 eV when a negative electric field of -1.0 V/Å was applied. This electric field dependence is three times larger than the one obtained for the  $CH_3^* \rightarrow CH_2^* + H^*$  reaction on the Ni(111) surface.<sup>34</sup> As for the results from Huang et. al.,<sup>20</sup> they added 1/2 ML Au on the Step-

edge of a Ni(211) surface and found that this decreased the energy barrier by 0.04 eV, which is a similar variation as compared to our negative electric field effect results. Overall, the electric field effect on this elementary  $CH_3^* \rightarrow CH_2^* + H^*$  reaction on the Ni(211) surface is as large as the one reported when 1/2 ML Au is deposited on a Ni(211) surface.

**Table 4.** Summary of the Energy Barriers of  $CH_x$  Species Dissociation on the Ni(211) Surface with and without an External Electric Field

Reaction pathways	Transition State	Energy Barriers (eV)	
		Ni(211)	Ni(111) <sup>34</sup>
$CH_3^* \rightarrow CH_2^* + H^*$	CH <sub>2</sub> (Sb), H (Sb)	0.677 / 0.627 (0.63 <sup>a</sup> , 0.65 <sup>b</sup> ) / 0.581	0.713 / 0.692 (0.798 <sup>c</sup> , 0.78 <sup>d</sup> ) / 0.680
$CH_2^* \rightarrow CH^* + H^*$	CH <sub>2</sub> (S4)	0.366 / 0.347 (0.41 <sup>a</sup> , 0.21 <sup>b</sup> ) / 0.451	0.349 / 0.323 (0.360 <sup>c</sup> , 0.37 <sup>d</sup> ) / 0.304
$CH^* \rightarrow C^* + H^*$	C (S4), H (SUb)	0.709 / 0.653 (0.62 <sup>a</sup> , 0.68 <sup>b</sup> ) / 0.596	1.494 / 1.373 (1.422 <sup>c</sup> , 1.36 <sup>d</sup> ) / 1.271

Energy barriers on Ni(211) in the presence of a positive electric field of 1.0 V/Å, in the absence of a field and with a negative electric field of -1.0 V/Å, respectively. Reference energy barrier values in the absence of a field are given in parentheses.

<sup>a</sup> from Ref. <sup>20</sup>; <sup>b</sup> from Ref. <sup>19</sup>; <sup>c</sup> from Ref. <sup>55</sup>; <sup>d</sup> from Ref. <sup>56</sup>

#### 3.4.2 Reaction Pathway: $CH_2^*(SUh1\_2) \rightarrow CH_2^*(Sb\_1) \rightarrow CH^*(s4) + H^*(SUh1)$

The next dissociation step of the methyl species is  $CH_2^* \rightarrow CH^* + H^*$ . The CH<sub>2</sub> molecule is initially adsorbed at the most stable SUh1\_2 site (Fig. 12A), with C-H bond lengths of 1.162 Å and 1.101 Å. Firstly, it shifted to the Sb site as a minimum intermediate with two barely equal C-H bond lengths of 1.105 Å and 1.099 Å (Fig. 12C). At the second TS (Fig. 12D), the CH<sub>2</sub> molecule shifted towards the S4 site with C-H bond lengths of 1.101 Å and 1.136 Å, suggesting that the C-H bond was still not broken at this state. For the final product, the bond length between the C atom and the leaving H atom is 3.524 Å. As in the previous case of a CH<sub>3</sub> molecule decomposition to form CH<sub>2</sub> and H species, this reaction pathway was calculated in two separate parts. The first part is  $CH_2^*(SUh1\_2) \rightarrow CH_2^*(Sb\_1)$  with an energy barrier of 0.067 eV and  $E_c$  of 0.064 eV. The energy barrier of the second part,  $CH_2^*(Sb\_1) \rightarrow CH^*(s4) + H^*(SUh1)$ , is 0.347 eV, which is 0.024 eV larger than the energy barrier of the  $CH_2^* \rightarrow CH^* + H^*$  reaction pathway on the Ni(111) surface.<sup>34</sup> A CH molecule adsorption at the S4 site with a H atom at the SUh1 site is the

final conformation of the reaction of  $CH_2^*(Sb\_1) \rightarrow CH^*(s4) + H^*(SUh1)$  on Ni(211), which significantly lowers the adsorption energy of the  $CH_2$  at  $SUh1\_2$  site by  $-0.644$  eV.

In addition, we also investigated the external electric field effect on this reaction. The energy barrier of the  $CH_2^*(Sb\_1) \rightarrow CH^*(s4) + H^*(SUh1)$  reaction was increased by  $0.019$  eV when a positive electric field of  $1.0$  V/Å was applied. It is worth mentioning that the energy barrier of the  $CH_2^*(Sb\_1) \rightarrow CH^*(s4) + H^*(SUh1)$  reaction also increased by  $0.104$  eV in the presence of the negative electric field, which differs to the results as obtained for the Ni(111) surface<sup>34</sup> since a negative electric field decreased the energy barrier in that case. The resulting increase of  $0.1$  eV in the presence of a negative electric field is also larger than the corresponding reaction on the Ni(111) surface or by adding  $1/2$  ML of Au to the step-edge surface on the Ni(211) surface.<sup>20</sup> This is most likely due to the stabilization of point C in the minimum energy pathway as given in Fig. 12. Interestingly, we also remark that the TS for the  $CH_2^*(Sb\_1) \rightarrow CH^*(s4) + H^*(SUh1)$  reaction has the  $CH_2$  molecule at the S4 site (Fig. 12D), but the other elementary reactions on the Ni(111) and Ni(211) surfaces have TS with one of the C-H bonds being broken.

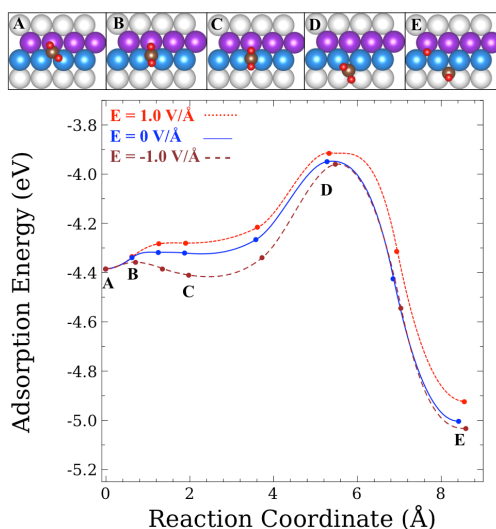


Fig. 12. The electric field effects on the minimum energy pathway of the reaction of  $CH_2^*(SUh1\_2) \rightarrow CH_2^*(Sb\_1) \rightarrow CH^*(s4) + H^*(SUh1)$ . The A-E images show the molecular structures along with this pathway.

### 3.4.3 Reaction Pathway: $CH^*(s4) \rightarrow C^*(s4) + H^*(s4) \rightarrow C^*(s4) + H^*(SUh1)$

The final step for the dissociation reaction of methyl species on the Ni(211) surface is  $CH^* \rightarrow C^* + H^*$ . The configuration of the reaction minimum intermediate had a H atom at a

nearby S4 site and a C atom at the original S4 site, with a C-H bond length of 2.702 Å. The final product is C at the original S4 site with a H atom at an adjacent SUh1 site, with a distance of 3.530 Å. For the  $CH^*(s4) \rightarrow C^*(s4) + H^*(s4)$  reaction, it has an energy barrier of 0.653 eV and a co-adsorption reaction energy of -0.071 eV, indicating this reaction is slightly exothermic. Moreover, the  $C^*(s4) + H^*(s4) \rightarrow C^*(s4) + H^*(SUh1)$  reaction further lowered the reaction energy by -0.307 eV, which is different from the  $CH^* \rightarrow C^* + H^*$  reaction on the Ni(111) surface with an endothermic reaction energy of 0.581 eV. This verifies that carbon deposits are much easier to form on the stepped Ni(211) surface, rather than the Ni(111) surface. For the TS in the  $CH^*(s4) \rightarrow C^*(s4) + H^*(s4)$  reaction, a H atom was at the SLb site with a C-H bond length of 1.477 Å which is 0.4 Å larger the regular C-H bond length in a CH molecule, suggesting that the C-H had been broken at the TS.

The external electric field effect on the  $CH^* \rightarrow C^* + H^*$  reaction is the similar to the  $CH_3^* \rightarrow CH_2^* + H^*$  reaction on the Ni(211) surface. When we introduced a positive electric field of 1.0 V/Å, the first energy barrier increased by 0.06 eV, relative to the case when no electric field is present, suppressing the CH molecules conversion to C atoms. The energy barrier decreased to 0.596 eV when a negative electric field of -1.0 V/Å was applied. When Huang et. al.<sup>20</sup> added 1/2 ML Au to the step-edge on a Ni(211) surface, the results showed that the energy barrier of  $CH^* \rightarrow C^* + H^*$  increased by 0.08 eV as compared the pure Ni(211) surface, which is slightly larger than our positive electric field effect results. However, the external electric field effect on the dissociation of a CH molecule on a Ni(111) surface<sup>34</sup> is twice as large as that on the Ni(211) surface.

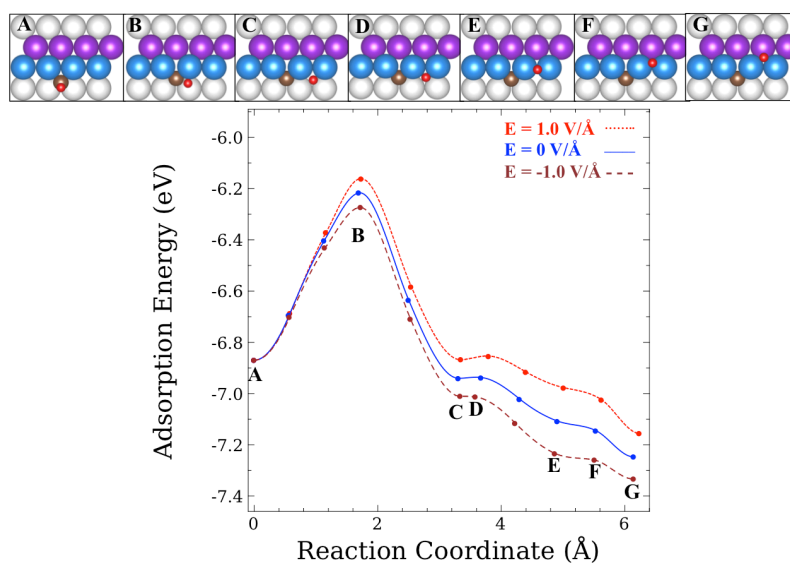
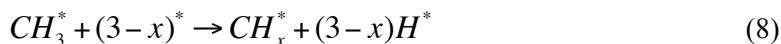


Fig. 13. The external electric field effects on the minimum energy pathway of  $CH^*(s4) \rightarrow C^*(s4) + H^*(s4) \rightarrow C^*(s4) + H^*(SUH1)$  reaction. The A-G images show the molecular configurations in this pathway.

### 3.4.5 Role of the electric field in methyl species dissociation

In order to recognize the role of the electric field in the decomposition reaction of methyl species on the Ni(211) surface, the potential energy diagrams of positive, negative and no electric fields are illustrated in Fig. 14, with a comparison of various Au/Ni surfaces.<sup>20</sup> The dissociation reaction energies ( $\Delta E_{diss}$ ) along with the pathways were defined and calculated by Eq. (8) and Eq. (9), which are shown as follows. Eq. (8) presents the dissociation reaction of  $CH_3^*$  adsorbates to form  $CH_2^*$  and  $H^*$ ,  $CH^*$  and  $2H^*$ ,  $C^*$  and  $3H^*$  species, where  $x$  is in the range of 1 to 3 and '\*' represents the metal slab. Here, we assume that the final state has the H atoms and the  $CH_x$  molecules at an infinite distance on the Ni(211) surface.



$$\Delta E_{diss} = [E_{(CH_x^*/slab)} + (3-x)E_{(H^*/slab)}] - [E_{(CH_3^*/slab)} + (3-x)E_{(slab)}] \quad (9)$$

The results from Fig. 14 (a) show that when a positive electric field of  $1.0 \text{ V/\AA}$  was applied, the adsorption energy of C and H species decreased by  $0.3 \text{ eV}$  via the reaction paths, indicating that a positive electric field impedes the formation of pure carbon atoms on the Ni(211) surface. On the other hand, from the results of Huang et. al.,<sup>20</sup> various alloy Au/Ni(211) surfaces can also suppress the carbon deposits on the Ni catalysts. However, the Au/Ni catalysts would be more expensive to prepare than the pure Ni catalysts and Au atoms can be easily sintered to form large Au particles.

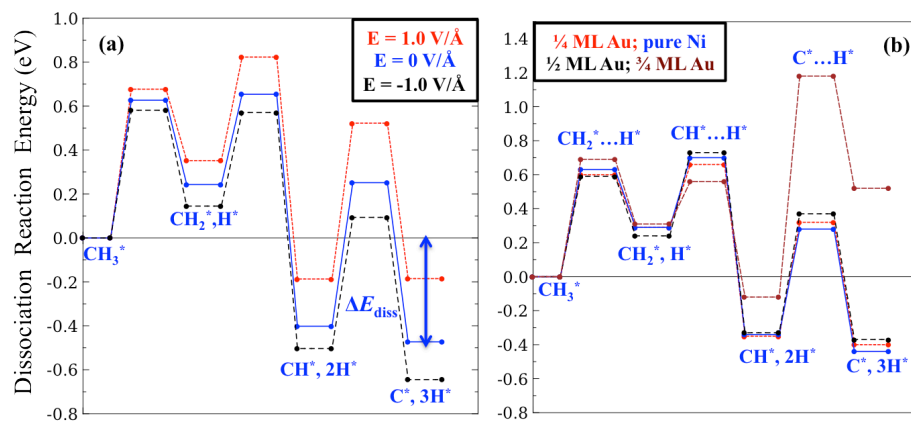
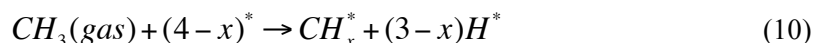


Fig. 14. The dissociation reaction energy of methyl species on Ni (211) in the presence of an external electric field, with a comparison of various Au/Ni (211) surfaces.<sup>20</sup> All the energies are relative to the adsorption energy of a CH<sub>3</sub> molecule on Ni(211).

It is also valuable to provide an overview picture of the methyl dissociation mechanism on the Ni(211) surfaces with and without an electric field, as shown in Fig. 15. Here we defined the reaction as Eq. (10) and the dissociation reaction energies were calculated by Eq. (11) ( $x = 1\sim 3$ ), which are slightly different from Eq. (8) and Eq. (9). In addition, when  $x$  equals 3, the dissociation reaction energy is the same as the adsorption energy of a CH<sub>3</sub> molecule on Ni(211).



$$\Delta E_{\text{diss}} = [E_{(\text{CH}_x/\text{slab})} + (3-x)E_{(\text{H}/\text{slab})}] - [E_{(\text{CH}_3/\text{gas})} + (4-x)E_{(\text{slab})}] \quad (11)$$

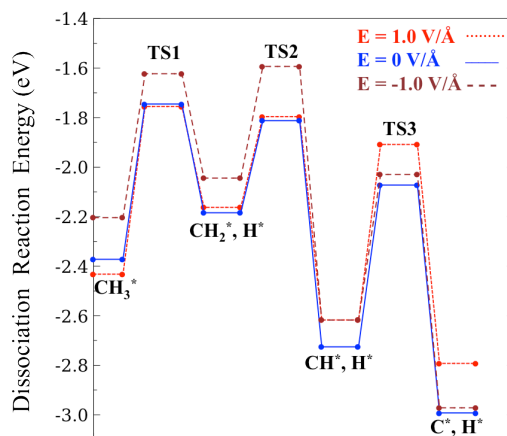


Fig. 15. The electric field effects on the reaction energy pathways of the CH<sub>3</sub> species decomposition to form the C\* and 3H\* species on the Ni (211) surface.

From the computed energy barriers in Table 4 and Fig. 15, the rate-limiting step of the CH<sub>3</sub> group dissociation on the Ni(211) surface is  $\text{CH}^* \rightarrow \text{C}^* + \text{H}^*$  with an energy barrier of 0.653 eV, which is only 0.026 eV larger than that of the  $\text{CH}_3^* \rightarrow \text{CH}_2^* + \text{H}^*$  reaction. The lowest energy barrier of these three elementary reactions was found to be the decomposition of a CH<sub>2</sub> molecule. Compared to reactions on the Ni(111) surface, the energy barriers of the  $\text{CH}_3^* \rightarrow \text{CH}_2^* + \text{H}^*$  and  $\text{CH}_2^* \rightarrow \text{CH}^* + \text{H}^*$  reactions are similar. However, the  $\text{CH}^* \rightarrow \text{C}^* + \text{H}^*$  reaction has an energy barrier of 1.373 eV on the Ni(111) surface,<sup>34</sup> which is a factor of two higher than that of Ni(211) surface, indicating that the rate-limiting step on the Ni(111) surface requires a greater activation

energy as compared to the Ni(211) surface. This also verifies that pure carbon atoms are more easily deposited on the stepped Ni(211) surface than the close-packed Ni(111) surface.

Generally, the CH<sub>3</sub> molecule adsorption at the Sb site goes through the TS1, which results in a CH<sub>2</sub> molecule and a H atom at their most stable sites with an infinite separating distance. Similarly, CH<sub>2</sub> and CH species pass through TS2 and TS3 transition states and generate isolated CH and H species followed by isolated C and H adsorbates. From Fig. 15, it is clear that the presence of an external electric field, in the order of -1.0 V/Å to 1.0 V/Å, has a significant effect on the energy barrier of the  $CH^* \rightarrow C^* + H^*$  reaction. It is also worthwhile to mention that a CH<sub>3</sub> molecule with a positive electric field of 1.0 V/Å has the most stable adsorption energy as compared to cases with a negative electric field and in the absence of an electric field. This CH<sub>3</sub> molecule in the presence of a positive field will also eventually go through the largest energy barrier to form C\* and 3H\* with weaker adsorption energies. Such conclusions are similar to the ones obtained on the Ni(111) surface. This suggests a positive electric field could hinder the pure carbon formation on the Ni catalysts for both flat and stepped surface structures.

#### 4. Conclusions

The influences of positive and negative external electric fields on the adsorption of isolated hydrocarbon species and the co-adsorption of CH<sub>x</sub> and H species on the Ni(211) surface were investigated using DFT calculations. For isolated hydrocarbon species, it was found that the C and H atoms have similar field effects, where positive electric fields weaken the adsorption energies much more than the negative ones. For the CH, CH<sub>2</sub> and CH<sub>3</sub> species, the electric field effects are opposite to the C and H atoms, where negative electric fields weaken the adsorption strength much more the positive field values. For the co-adsorption of CH<sub>x</sub> and H species, the co-adsorption reaction energies increase monotonically when the electric field increases from -1.0 V/Å to 1.0 V/Å. When comparing these results with the species adsorbed on the Ni(111) surface,<sup>34</sup> the adsorbates adsorbed more strongly on the Ni(211) surface. In addition, we found that the different adsorption sites of the Ni(211) surface have different local electric field distributions ΔF.

The minimum energy pathways of the methyl species decomposition to form C and H species on the Ni(211) surface in the presence and absence of an external electric field were examined as well. For the  $CH_3^* \rightarrow CH_2^* + H^*$  and the  $CH^* \rightarrow C^* + H^*$  reactions, a positive electric field could increase the energy barriers hindering the dissociation of the methyl species and a negative electric field could decrease the energy barriers, which is similar to the effects presented on the Ni(111) surface. On the other hand, both positive and negative electric fields increase the

energy barriers in the  $CH_2^* \rightarrow CH^* + H^*$  reaction. Importantly, the electric field effects on the energy barriers of these three elementary decomposition reactions are similar to the addition of 1/2 ML Au on Ni(211).<sup>20</sup> In addition, a  $CH_3$  molecule will go through the highest energy barrier to form weakly bound C and H atoms when a positive electric field is applied. As a result, pure carbon atoms will not strongly adhere to the catalyst surface for positive field values as compared to when it is absent. Consequently, the application of a positive electric field can directly decrease the number of pure carbon atoms on a Ni(211) surface when exposed to methane resulting in a suppression in the formation of coke.

## 5. Acknowledgments

This work was supported by institutional funds provided to JSM from the Voiland School of Chemical Engineering and Bioengineering and by the American Chemical Society Petroleum Research Fund under grant number 52769-DNI5. We acknowledge computational resources provided by the Center for Nanoscale Materials at Argonne National Laboratory. Use of the Center for Nanoscale Materials was supported by the U. S. Department of Energy, Office of Science, Office of Basic Energy Sciences, under Contract No. DE-AC02-06CH11357. We also thank Dr. Renqin Zhang for helpful discussions and comments.

## References

- (1). S. C. Singhal, *Solid State Ionics*, 2000, **135**, 305-313.
- (2). E. Nikolla, J. Schwank, S. Linic, *J. Electrochem. Soc.*, 2009, **156**, B1312-B1316.
- (3). W. Wang, W. Zhou, R. Ran, R. Cai, Z. Shao, *Electrochem. Commun.*, 2009, **11**, 194-197.
- (4). S. Park, J. M. Vohs, R. J. Gorte, *Nature*, 2000, **404**, 265-267.
- (5). Y. Lin, Z. Zhan, J. Liu, S. Barnett, *Solid State Ionics*, 2005, **176**, 1827-1835.
- (6). B. C. H. Steele, *Nature*, 1999, **400**, 619-621.
- (7). S. Rakass, H. Oudghiri-Hassani, P. Rowntree, N. Abatzoglou, *J. Power Sources*, 2006, **158**, 485-496.
- (8). M. Dokiya, *Solid State Ionics*, 2002, 383-392.
- (9). J. Meusinger, E. Riensche, U. Stimming, *J. Power Sources*, 1998, **71**, 315-320.
- (10). H. Koide, Y. Someya, T. Yoshida, T. Maruyama, *Solid State Ionics*, 2000, **132**, 253-260.
- (11). N. F. P. Ribeiro, M. M. V. M. Souza, O. R. M. Neto, S. M. R. Vasconcelos, M. Schmal, *Appl. Catal., A: General*, 2009, **353**, 305-309.
- (12). E. S. Hecht, G. K. Gupta, H. Zhu, A. M. Dean, R. J. Kee, L. Maier, O. Deutschmann, *Appl. Catal., A: General*, 2005, **295**, 40-51.
- (13). M. Vandenbossche, S. McIntosh, *J. Catal.*, 2008, **255**, 313-323.
- (14). R. Oza, S. Patel, *Res. J. Recent Sci.*, 2012, **1**, 434-443.
- (15). T. V. Choudhary, D. W. Goodman, *J. Mol. Catal. A: Chem.*, 2000, **163**, 9-18.
- (16). M. Shishkin, T. Ziegler, *J. Phys. Chem. C*, 2008, **112**, 19662-19669.
- (17). H. S. Bengaard, J. K. Nørskov, J. Sehested, B. S. Clausen, L. P. Nielsen, A. M. Molenbroek, J. R. Rostrup-Nielsen, *J. Catal.*, 2002, **209**, 365-384.
- (18). W. An, X. C. Zeng, C. H. Turner, *J. Chem. Phys.*, 2009, **131**, 174702.
- (19). Y. Xu, C. Fan, Y. A. Zhu, P. Li, X. G. Zhou, D. Chen, W. K. Yuan, *Catal. Today*, 2012, **186**, 54-62.
- (20). Y. C. Huang, J. Y. Du, C. Y. Ling, T. Zhou, S. F. Wang, *Cat. Sci. Technol.*, 2013, **3**, 1343-1355.
- (21). J. H. Jeong, J. W. Lee, D. J. Seo, Y. Seo, W. L. Yoon, D. K. Lee, D. H. Kim, *Appl. Catal., A: General*, 2006, **302**, 151-156.
- (22). H. Arbag, S. Yasyerli, N. Yasyerli, G. Dogu, *Int. J. Hydrogen Energy*, 2010, **35**, 2296-2304.
- (23). S. Takenaka, Y. Shigeta, E. Tanabe, a. K. Otsuka, *J. Phys. Chem. B*, 2004, **108**, 7656-7664.
- (24). M. García-Diéguez, I. S. Pieta, M. C. Herrera, M. A. Larrubia, L. J. Alemany, *J. Catal.*, 2010, **270**, 136-145.
- (25). L. Pleth Nielsen, F. Besenbacher, I. Stensgaard, E. laegsgaard, *Phys. Rev. Lett.*, 1993, **71**, 754-759.
- (26). M. M. Hatlo, R. v. Roij, L. Lue, *Europhys. Lett.*, 2012, **97**, 28010.
- (27). E. M. Stuve, *Chem. Phys. Lett.*, 2012, **519-520**, 1-17.
- (28). R. M. Ormerod, *Chem. Soc. Rev.*, 2003, **32**, 17-28.
- (29). G. S. Karlberg, J. Rossmeisl, J. K. Nørskov, *Phys. Chem. Chem. Phys.*, 2007, **9**, 5158-5161.
- (30). J. Zhang, A. Yu, V. Chabot, Z. Chen, *Electrochemical Supercapacitors For Energy Storage And Delivery: Fundamentals And Applications*. CRC PRESS INC: US, 2013; p 39-96.
- (31). Y. Sekine, M. Haraguchi, M. Tomioka, M. Matsukata, E. Kikuchi, *J. Phys. Chem. A*, 2009, **114**, 3824-3833.
- (32). Y. Sekine, M. Tomioka, M. Matsukata, E. Kikuchi, *Catal. Today*, 2009, **146**, 183-187.
- (33). Y. Sekine, M. Haraguchi, M. Matsukata, E. Kikuchi, *Catal. Today*, 2011, **171**, 116-125.
- (34). F. Che, R. Zhang, A. J. Hensley, S. Ha, J.-S. McEwen, *Phys. Chem. Chem. Phys.*, 2014, **16**, 2399-2410.

- (35). M. C. Payne, T. A. Arias, J. D. Joannopoulos, *Rev. Mod. Phys.*, 1992, **64**, 1045-1097.
- (36). G. H. Golub, D. P. O'Leary, *J. Soc. Ind. Appl. Math.*, 1989, **31**, 50-102.
- (37). J. White, D. Bird, *Phys. Rev. B*, 1994, **50**, 4954-4957.
- (38). J. P. Perdew, K. Burke, M. Ernzerhof, *Phys. Rev. Lett.*, 1996, **77**, 3865-3869.
- (39). J. P. Perdew, Y. Wang, *Phys. Rev. B*, 1992, **45**, 13244-13249.
- (40). S. G. Louie, S. Froyen, M. L. Cohen, *Phys. Rev. B*, 1982, **26**, 1738-1742.
- (41). D. F. Shanno, *Math. Comp.*, 1970, **111**, 647-655.
- (42). H. Orita, N. Itoh, Y. Inada, *Surf. Sci.*, 2004, **571**, 161-172.
- (43). H. J. Monkhorst, J. D. Pack, *Phys. Rev. B*, 1976, **13**, 5188-5192.
- (44). K. Christmann, R. J. Behm, G. Ertl, M. A. Van Hove, W. H. Weinberg, *J. Chem. Phys.*, 1979, **70**, 4168-4184.
- (45). H. Jonsson, G. Mills, K. W. Jacobsen, *Nudged elastic band method for finding minimum energy paths of transitions*. 1998; Vol. 16, p 385.
- (46). G. Henkelman, H. Jonsson, *J. Chem. Phys.*, 1999, **111**, 7010-7023.
- (47). G. Henkelman, B. P. Uberuaga, H. Jonsson, *J. Chem. Phys.*, 2000, **113**, 9901-9904.
- (48). S. A. Trygubenko, D. J. Wales, *J. Chem. Phys.*, 2004, **120**, 2082-2094.
- (49). G. Henkelman, A. Arnaldsson, H. Jonsson, *J. Chem. Phys.*, 2006, **124**, 044706.
- (50). R. C. Catapan, A. A. M. Oliveira, Y. Chen, D. G. Vlachos, *J. Phys. Chem. C*, 2012, **116**, 20281-20291.
- (51). J. S. McEwen, P. Gaspard, T. Visart de Bocarmé, N. Kruse, *J. Phys. Chem. C*, 2009, **113**, 17045-17058.
- (52). Y. Zhao, S. Li, Y. Sun, *Chinese J. Catal.*, 2013, **34**, 911-922.
- (53). R. Zhao, S. J. Lee, I. H. Son, H. Lee, A. Soon, *Appl. Surf. Sci.*, 2013, **265**, 339-345.
- (54). Y. Suchorski, W. A. Schmidt, N. Ernst, J. H. Block, H. J. Kreuzer, *Prog. Surf. Sci.*, 1995, **48**, 121-134.
- (55). J. E. Mueller, A. C. T. van Duin, W. A. Goddard, *J. Phys. Chem. C*, 2009, **113**, 20290-20306.
- (56). H. Y. Liu, R. X. Yan, R. G. Zhang, B. J. Wang, K. C. Xie, *J. Nat. Gas Chem.*, 2011, **20**, 611-617.